Developments in the Built Environment 25 (2026) 100855

Contents lists available at ScienceDirect

Developments in the Built Environment

journal homepage: www.sciencedirect.com/journal/developments-in-the-built-environment

Using single sided ^{1}H nuclear magnetic resonance to investigate water absorption and stability of earth-based building materials

Florian Soßna [a,*], Robert Schulte Holthausen [b], Jeanette Orlowsky [a]

[a] Department of Building Materials, TU Dortmund University, August-Schmidt-Str. 8, Dortmund, 44227, Germany
[b] Technische Hochschule Mittelhessen University of Applied Sciences, Wiesenstrasse 14, Gießen, 35390, Germany

ARTICLE INFO

To be submitted to *Developments in the Built Environment*, Special Issue *Cutting-Edge Testing and Data Analytics for Constructional Materials*

Keywords:
Earthen material
Earthen blocks
^{1}H nuclear magnetic resonance
Capillary water absorption

ABSTRACT

There is an increasing interest in the use of earth-based building materials to improve the environmental footprint of our built environment. One of the crucial features currently limiting its use is the inferior resistance of the clay binder to water absorption and erosion. Furthermore, there is a lack of meaningful quantitative measurement methods for characterising earthen material as building material.

Here, we study the water absorption into earth-based materials with ^{1}H single-sided nuclear magnetic resonance. Samples are prepared using an elaborate extrusion process and preconditioned under several typical moisture conditions. We demonstrate the use of the ^{1}H NMR technique to visualize the water absorption and to quantify the capillary water absorption. The latter increases with a more water-reducing preconditioning. Furthermore, the technique allows for the visualisation of the internal swelling of the clay binder, illustrating the strong influence of sample preconditioning.

1. Introduction

1.9 tons per capita – this quantity of construction and demolition waste was generated in the European Union in 2022 (eurostat, 2022). There are continuous efforts to reduce these amounts of waste and promote the reuse and recycling. One possibility is the use of earth-based materials in construction. Besides other advantages, these materials are readily available throughout Europe and can be easily recycled without a heating process, resulting in a high recycling potential (Calatan et al., 2017). This recycling potential is simultaneously a disadvantage in terms of moisture behaviour. The compressive strength of unstabilized earth materials decreases in correlation with higher humidity. When exposed to direct weathering, the material loses its cohesive properties and dissolves in water. These characteristics can be summarized under the notion of replastification of earthen blocks and building materials.

The speed and degree of replastification depend primarily on the clay minerals present and secondarily on the pore structure of the earth block. Clay minerals are phyllosilicates in a two or three-layer arrangement of tetrahedral and octahedral sheets. Depending on the charge density of the layers, some clay minerals adsorb water in their interlayer space (Kumari et al., 2021). This adsorption of water molecules leads to an increase in the interlayer space from 10, up to 20 Å, while maintaining their quasi-crystalline order. An increase above 20 Å, resulting from the accumulation of more water molecules, leads to the separation of the clay layers with diffuse ion layers in between (Jasmund and Lagaly, 1993).

For the described swelling to occur, free water must be available in proximity to the clay particles. While free water in direct contact with the surface leads to swelling of the clay minerals, it must be conducted deeper into the earthen block through capillary pores to lead to swelling in greater depths. The conveyance can be described using e.g. the model of Rose (1965).

To address the issue of replastification, various constructive and regulatory measures were implemented in the German construction sector over the last years. One of those regulations concerns the base of walls out of earth blocks. To prevent capillary suction in the event of water damage, every wall made of earth blocks needs to be placed on a base that rises 5 cm above the top edge of the floor. This base must be made of hydraulically bound or fired material (DIN 18940: 2023-06).

This article is part of a special issue entitled: Novel Materials Testing published in Developments in the Built Environment.

* Corresponding author.
E-mail addresses: florian.sossna@tu-dortmund.de (F. Soßna), robert.schulte.holthausen@bau.thm.de (R.S. Holthausen), jeanette.orlowsky@tu-dortmund.de (J. Orlowsky).

https://doi.org/10.1016/j.dibe.2026.100855
Received 29 June 2025; Received in revised form 13 January 2026; Accepted 14 January 2026
Available online 17 January 2026

Another regulation relates to exposure to weathering. Earthen blocks must be classified in one of three application classes (AK) by the manufacturer, which determines whether the bricks can be used as plastered exterior masonry exposed to weathering (AKIb) or interior masonry (AKIII). To classify, the bricks must fulfil various criteria for geometry and moisture behaviour, such as immersion tests, contact tests, suction tests, and frost tests (DIN 18945: 2024-04). Except for the immersion test, all other methods mentioned heavily rely on visual inspection of cracking and swelling deformation and thus are subjective criteria. For a wider use of earthen materials, more quantitative methods are essential.

To characterise the behaviour of earthen blocks at different humidity levels and in direct contact with water, proton nuclear magnetic resonance (^{1}H NMR) measurements appear predestined. ^{1}H NMR is a highly effective technique for investigating the behaviour of water in porous materials. This method leverages quantum-mechanical interactions between the nuclear spin of protons, that are abundant in water-saturated building materials, and their interactions with surrounding solid surfaces. In this approach, hydrogen spins are initially aligned within a constant magnetic field, causing them to precess at the so-called Larmor frequency. By emitting electromagnetic pulses at this resonance frequency, the spins are excited and rotated away from their equilibrium orientation, enabling the detection of an electromagnetic response. In inhomogeneous magnetic fields, variations in field strength lead to differences in precession frequencies, resulting in rapid dephasing of the spin ensemble and a consequent loss of signal. To counteract this effect, the Carr–Purcell–Meiboom–Gill (CPMG) pulse sequence (Carr et al., 1954; Meiboom et al., 1958) is employed. This sequence repeatedly refocuses the spins, generating a series of spin echoes that can be measured over time. Two key parameters can be independently extracted from the CPMG signal. The initial signal amplitude corresponds to the proton density, while the subsequent exponential decay, characterised by the transverse relaxation time T_2, reflects proton mobility. In the fast diffusion regime, as described by Brownstein and Tarr (1979), a direct proportionality exists between the T_2 relaxation time and the characteristic size of the pores as:

$$\frac{1}{T_2} = \frac{f_B}{T_{2B}} + \frac{f_s}{T_{2s}} \approx \frac{S_p}{V_p}\frac{\varepsilon_s}{T_{2s}} \approx \frac{2\lambda}{d} \quad \text{Eq. 1}$$

Here, T_2 is the detected relaxation time, f_b and f_s are the volume fractions of water of the bulk of the pore and within direct proximity to the pore wall surface, respectively, with its associated T_2 relaxation times. Surface relaxation is only effective in a very limited layer thickness ε_s, usually assumed to be only 0.28–0.5 nm, but shorter by several orders of magnitude compared to bulk relaxation. Thus, the overall detected relaxation is governed by surface relaxation and the bulk term can be neglected for most cases. Consequently, the contributing relaxation components can be rewritten in terms of the inner pore surface S_P and the total pore volume V_P. As ε_s and T_{2s} are combined into the surface relaxivity λ, the pore diameter d can be directly related to the relaxation time.

Past NMR studies on clays have described a multi-modal relaxation response, gaining deeper insight into the complex hydrated porous structure. Most studies describe a shortest relaxation component of well below 0.1 ms being assigned to closely bound hydroxyls within the clay interlayer structure (Fleury et al., 2013). Second, a very prominent signal is detected with a relaxation time of between 0.2 ms in dried clay, continuously extending to about 3 ms with increasing moisture content (Eizaguirre et al., 2024). As shown by NMR cryo porosimetry (Fleury et al., 2013), this signal not only comprises of interlayer water but includes water within larger interparticle spaces. Due to the high mobility and fast exchange of water molecules, the relaxation components of these two pore spaces merge and average out in the NMR equipment employed with the overall relaxation time being mostly governed by the faster component.

Concerning the possible use of the conversion from relaxation time to pore size based on the fast diffusion regime, there is on-going discussion, how this applies to the range of relaxation times found in clay. Fleury et al. (2013) found a good correlation between basal distance, and thus water content, and smaller T_2 relaxation times that does not hold up for larger basal distances and thus longer relaxation times. They suggested that a closer relation between relaxation rate (inverse relaxation time) and basal distance describes the data best. More recently, Eizaguirre et al. (2024) suggested a two-regime process with individual contributions to the overall relaxation. The limiting water content between these regions was found to be of 30 %.

In this study, single-sided proton nuclear magnetic resonance is used on unstabilized earth-based building materials to gain deeper insights into water binding and swelling behaviour. Based on these measurements, important engineering properties are deduced, including water content and capillary water absorption.

2. Materials and methods

2.1. Experimental design

To investigate the water absorption and stability of earth blocks, three different samples are produced using a vacuum extruder. These samples are dried and conditioned at various temperatures and relative humidities (RH) according to the procedure shown in Fig. 1. The sample nomenclature and dimensions are listed in Table 1. Besides the ^{1}H nuclear magnetic resonance measurements on preconditioned samples and a dissolution test of those, conventional testing methods are performed, including water absorption, compression testing and mercury porosimetry. Additionally, to thoroughly characterise the material examined, a thermogravimetric analysis is done, the loss of ignition is determined and x-ray diffractometry is performed.

2.2. Earth-based materials used and sample production

2.2.1. Raw material characterisation

To characterise the earthen material used, loss of ignition and X-ray diffraction analysis are performed, in addition to a thermogravimetric analysis (TGA). These examinations are necessary due to its natural variability depending on the extraction site and the thickness of the clay layer.

The earthen material used for the blocks examined in the following section originates from the Midwest region of Germany. It is extracted from various pits throughout this area, each with its unique composition, colour, and processability. The material is homogenised at the pit, if necessary, and then transported to the brickwork for further homogenization, mixture with cellulose fibres, and production. The material used for the examined block samples is taken from the site after preprocessing, which involves crushing it down through a mill. The cellulose as well as natural organic inclusions can influence the water absorption of the extruded blocks; therefore, this parameter must be measured directly.

To gather information about inclusions within the earthen material, 20 mg probes are measured using the TGA/DSC3+ from Mettler Toledo. The probes are collected from an untested, extruded block and crushed using a mortar until the largest grain measures a diameter of less than 2 mm. The experiment is performed with a heating rate of 3 K/min, with holding times at 105 °C and 550 °C, where the temperature remains steady for 10 min each. The final temperature is reached at 920 °C, while the change in mass is monitored over time (see Fig. 2). The remaining water is expelled, resulting in a mass change of 0.9 wt.-%. The loss of mass between 105 °C and 550 °C is 4.4 wt.-%. The loss of ignition test in conclusion to EN 17685-1 (DIN EN, 17685-1: 2023–04) confirms these results.

Between 550 °C and 700 °C, carbonate derivatives dehydroxylate. Above this temperature, the mass loss continues at a much lower rate.

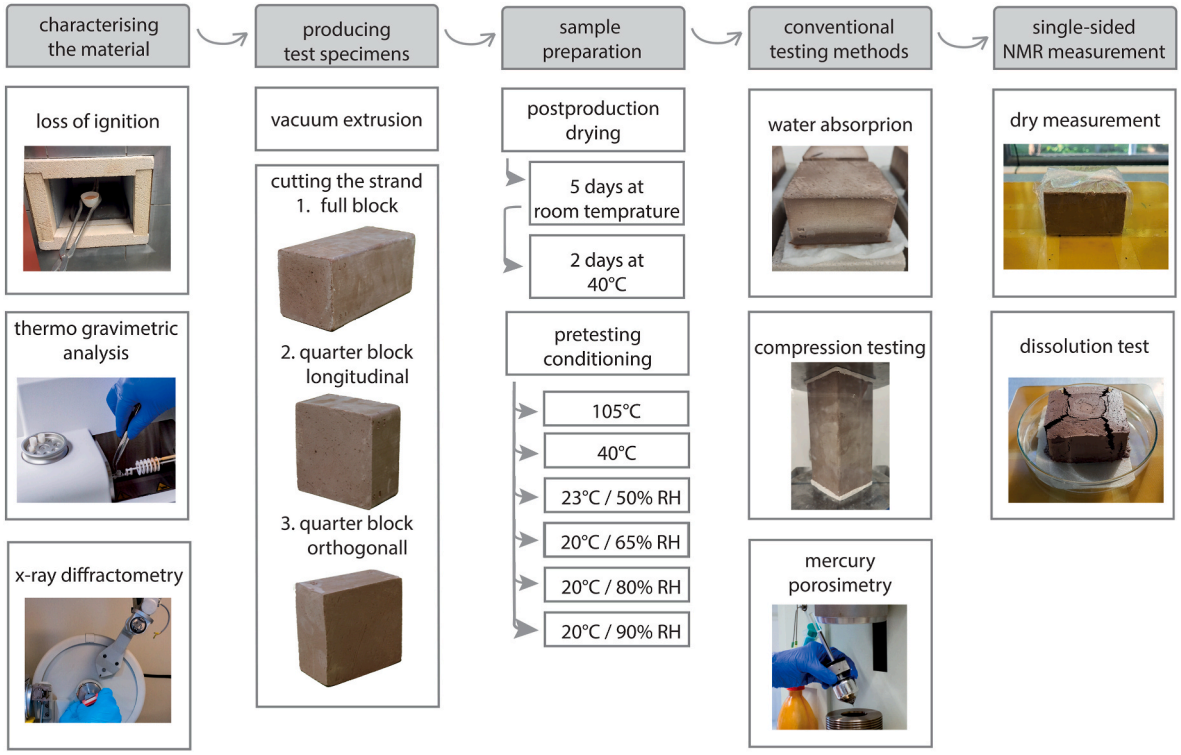

Fig. 1. Experimental flowchart.

Table 1
Nomenclature of samples used.

Sample No.	Sample orientation	a [mm]	b [mm]	h [mm]
0-1 to 0-15	full block	90	90	180
0-16 to 0-25	quarter block longitudinal (L)	90	90	45
0-26 to 0-35	quarter block orthogonal (O)	90	45	90

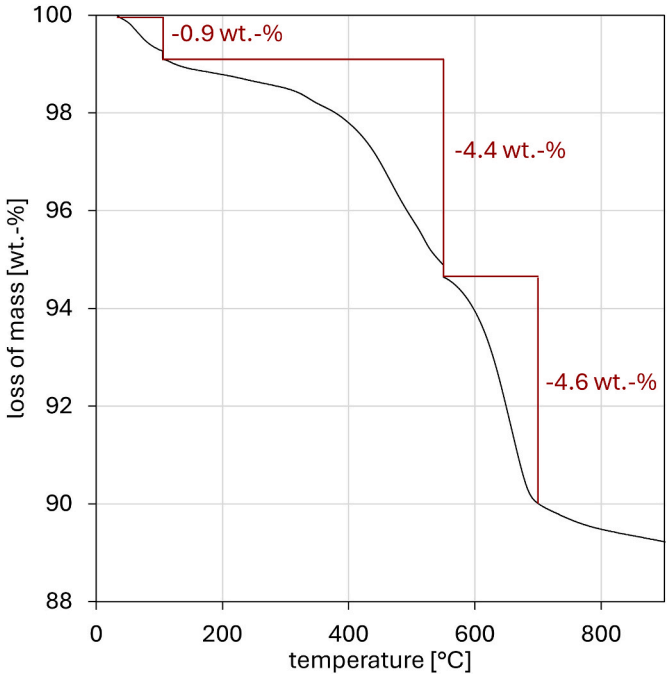

Fig. 2. Mass loss of the earthen material used by TGA from 25 °C to 910 °C.

This can be explained by carbonate decomposition (Chauhan et al., 2020).

Additionally, the structural analysis of the earthen material is performed using X-ray diffraction with a D8 Advanced Diffractometer by Bruker Co. The sample material is collected from compression-tested blocks and crushed using a pestle mortar. The prepared powder is pressed onto an aluminium oxide sample holder and transferred into the x-ray diffractometer. The samples are irradiated with focused X-rays at an angle θ. As the X-rays interact with the atomic lattice of the materials, they create characteristic reflection angles. These angles provide information about the components within the powder, allowing for the identification of the present mineral. Fig. 3 shows the diffractogram of the earthen material used in this study. The reflections indicate the presence of four common minerals. Muscovite and Kaolinite as clay minerals ensure the plasticizing behaviour through the addition of water while, in dry state ensuring the bonding of the aggregates in the earthen block. The aggregates consist of quartz and dolomite which are also shown by X-ray diffractometry.

Last, as the amount of paramagnetic impurity is of greater importance to NMR studies, the amount of iron oxide present within the samples is estimated to around 6 wt.-%. This estimate is derived from the chemical analysis of the raw clays provided by the manufacturer, along with the material mixture.

2.2.2. *Production of samples*

The production method is crucial for the material parameters of the earthen blocks. The raw material described in section 2.1.1 is earth-moist when delivered from the manufacturer to the Institute for Brick and Tile Research Essen, where the samples are extruded. First, to achieve a homogeneous and low-moisture level throughout the raw material, it is dried at 40 °C for several days. The production starts with this dried material, which is mixed with water. The consistency is then tested with a Pfefferkorn device (Göhlert et al., 2007) until a remaining height of 2.7 mm is reached. Consistency is crucial for vacuum extrusion moulding since material that is too soft or too solid results in incomplete extrusions and damaged samples. After mixing, the materials are filled

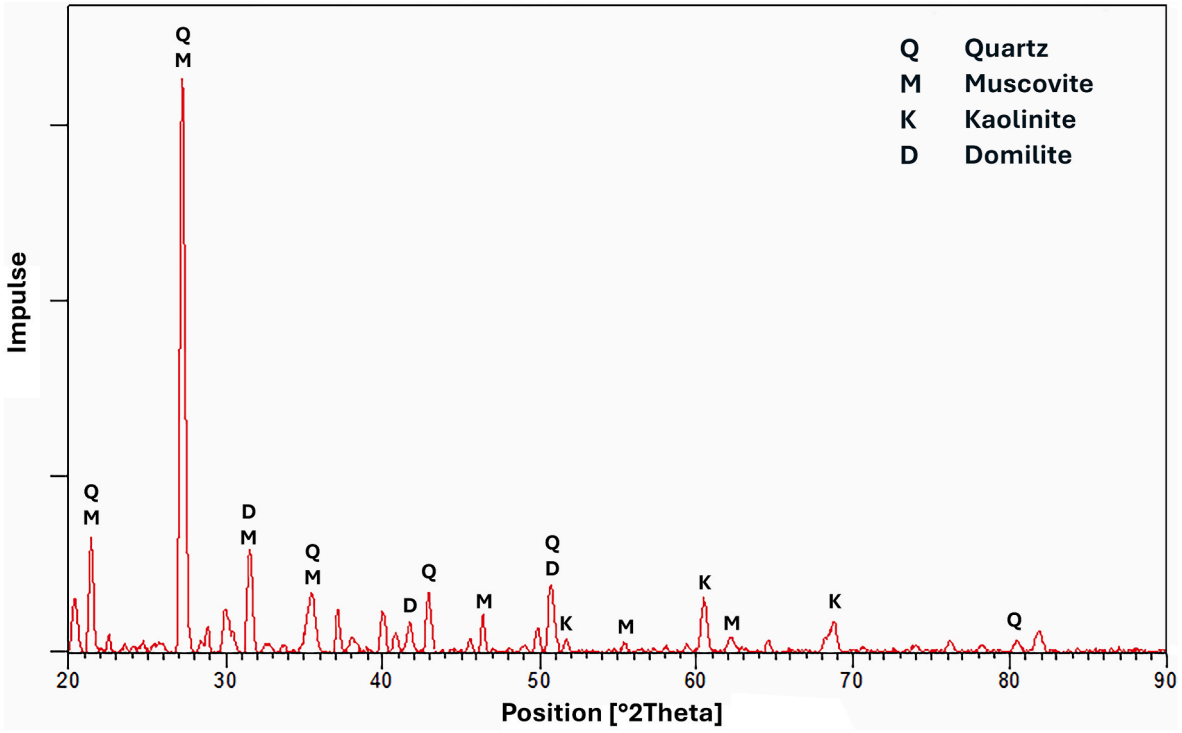

Fig. 3. Diffractogram of the earthen material used.

into a laboratory-sized vacuum extruder shown in Fig. 4.

The extrusion takes place at a pressure of 0.5 MPa, creating a monolithic strand with a dense, de-aired matrix (Bender and Händle, 2007) that measures 90 mm in height and thickness. Shortly after, the blocks are cut using a harp of tensioned wire. Three different samples are formed using different orientations of the cuts, as displayed in Fig. 5. First, samples with a length of 180 mm are cut off the strand for compression tests. Second, panes of 45 mm are cut for NMR testing along the pressing direction. Third, blocks of 90 mm are cut from the strand. These blocks are then cut into two smaller pieces, each with a thickness of 40 mm and 50 mm. The cut is placed along the pressing direction, creating samples for NMR testing orthogonal to the pressing direction.

After production, the samples are stored at room temperature on metal grids for several days, enabling gentle and slow drying. To finish the drying process, the samples are rearranged in an oven at 40 °C for two days.

Vacuum extrusion allows the production of earthen blocks on an industrial scale. The method used yields a steady quality, similar to other

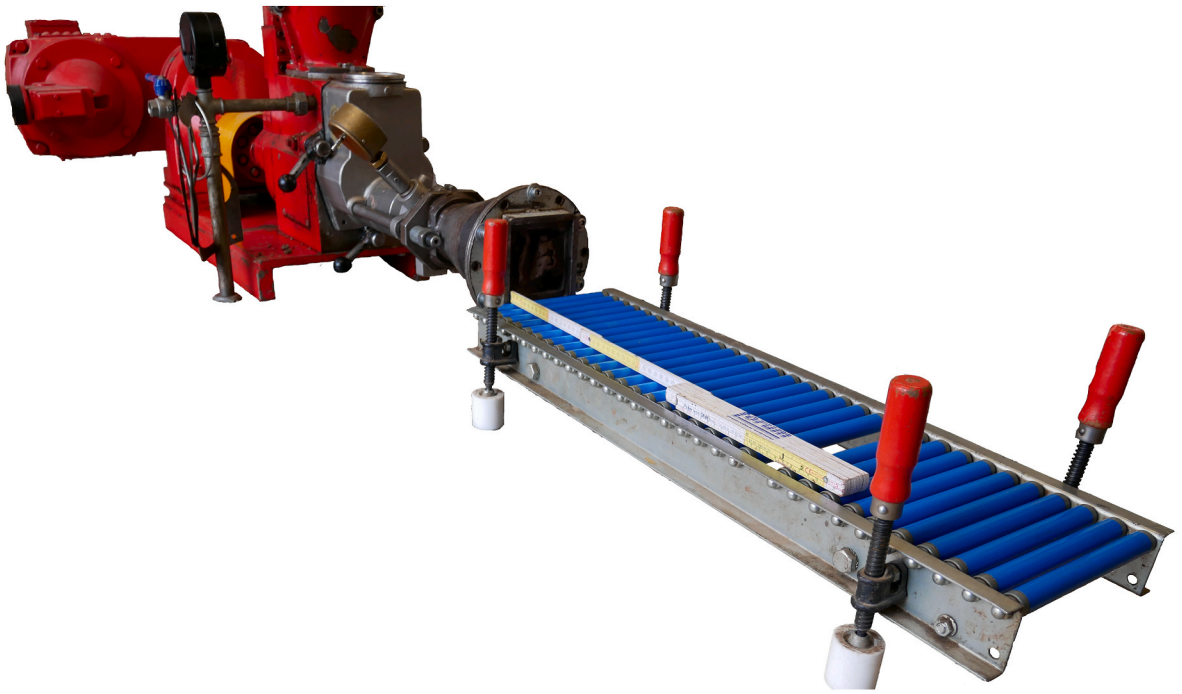

Fig. 4. Laboratory-sized vacuum extruder.

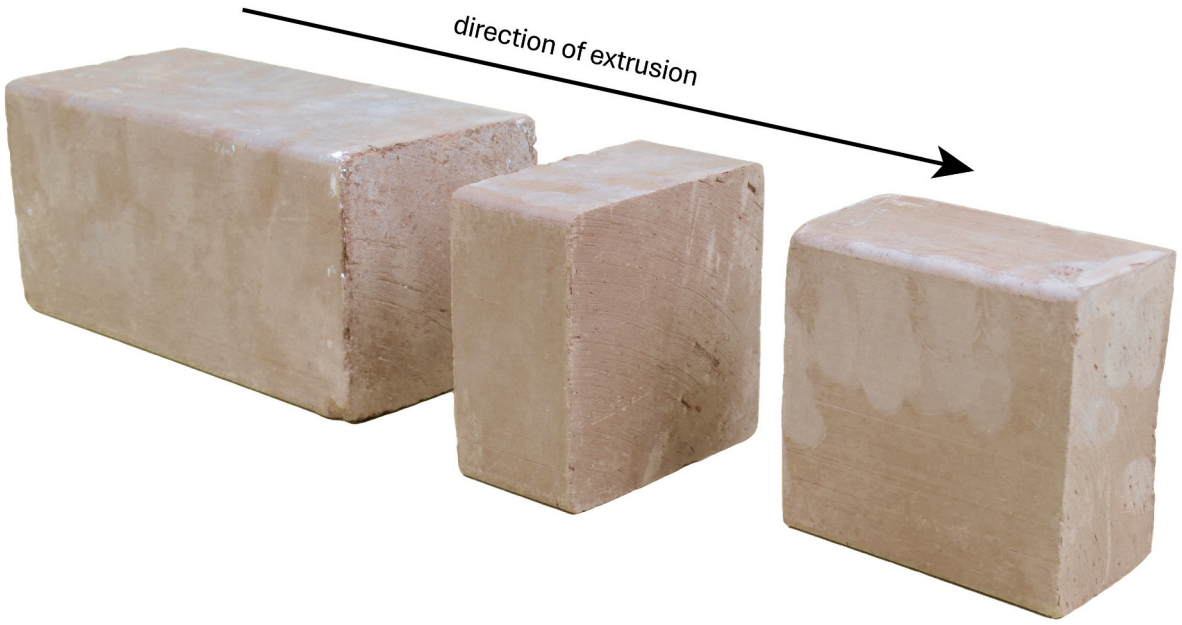

Fig. 5. Samples for compression tests (left, Sample 01–15), NMR-tests longitudinal (middle, Sample 16–25) and orthogonal (right, Sample 26–35) to the direction of extrusion.

types of masonry (Müller et al., 2013). At the same time, the infrastructure needed to produce vast quantities of earthen blocks already exists. Brickworks already produce earthen bricks, apart from the subsequent burning of the bricks (Berker et al., 2025). To work economically, the earthen material for most brickworks is excavated locally, thereby reducing costs and emissions from transportation at the same time (Soβna and Orlowsky, 2025).

2.2.3. *Conditioning of samples*

To investigate the influence of humidity on the earthen bricks in various climates, samples are preconditioned at climates of either 105 °C (105-XX), 40 °C (40-XX), 23 °C and 50 % RH (23–50), 20 °C and 65 % RH (20–65), 20 °C and 80 % RH (20–80) or 20 °C and 90 % RH (20–90). Samples are stored for a minimum of 28 days within the climates to generate a homogenous humidity within the samples. At this time, they are only taken from the climate to be weighed once a week.

Fig. 6. Experimental setup for capillary water absorption testing.

2.3. Conventional testing methods

2.3.1. Capillary water absorption

The experiment to determine the capillary water absorption is performed in accordance with (b) and (DIN EN, 15801: 2010–04). Before testing, the samples are stored in climates of 23 °C/65 % RH, 23 °C/50 % RH, and 40 °C for 4 weeks, during which they reached a constant mass with a difference of less than 0.5 % within seven days of storage. The earthen samples lay on sponge cloths, which themselves lay on top of capillary conductive sand-lime bricks. These are soaked with water and lay on line bearings in a tray, filled with water just 1–5 mm below the top side of the sand-lime bricks. The experimental setup described is shown in Fig. 6. In addition to monitoring cracks and swelling, as required in (b), the samples' weight is measured by removing the samples from the wet cloth after 15, 30, 60, 120, 180 min and 24 h. The water absorption is determined by Equation (2) (DIN EN, 15801: 2010–04).

$$Q = \frac{(m_i - m_0)}{A} \quad \text{Eq. 2}$$

The capillary water absorption coefficient C is determined as the secant slope of the water absorption over time, by the formular in Equation (3).

$$C = \frac{(m_i - m_0)}{A \cdot \sqrt{t}} = Q \cdot \frac{1}{\sqrt{t}} \quad \text{Eq. 3}$$

2.3.2. Compression testing

To evaluate the changes in compressive strength due to the differing humidity, three samples out of every climate mentioned in Fig. 1 are tested in a combined Compression/Bending Testing Machine 600 kN/30 kN by TESTING Bluhm & Feuerhardt GmbH, Berlin, Germany. Before testing, each sample is levelled with plaster and then again stored in the conditioning climate until constancy in mass is reached. The loading rate is 0.05 N/mm^2/s (DIN EN and 772-1, 2016–05) so that the maximum load is reached after 30–90 s in accordance with (b). The water content is calculated relative to the sample dried at 105 °C and after reaching a change of mass smaller than 0.5 % within seven days.

2.3.3. Mercury porosimetry

To obtain more detailed information about the pore distribution, fragments of samples are tested using mercury porosimetry. For this, a PASCAL 240 Series by Thermo Fischer Scientific, formerly Thermo-Quest, Waltham, United States of America, is used. The tested fragments are obtained by breaking an untested sample into smaller parts measuring about 7 mm in length and 4 mm in diameter. These Fragments are then cleaned of remaining dust particles with compressed air and dried at 40 °C until a constant mass is reached. The drying process is carried out as gentle as possible, so the samples and temperature sensitive components are not influenced.

2.4. ^1H single sided nuclear magnetic resonance

In this study, a single-sided ^{1}H nuclear magnetic resonance device called Mobile Universal Surface Explorer (NMR-MOUSE PM 25) is used (Blümich, 2000; Casanova et al., 2011), which enables the detection of NMR signal from a flat sensitive volume of roughly 50 x 50 × 0.2 mm outside the device, as shown in Fig. 7. The sensitive volume is produced by four permanent block magnets within the probe head. They are in perfect arrangement to produce an almost entirely flat region of the magnetic field, floating about 15 mm above the measurement probe head. Within this sensitive volume, hydrogen spins are excited through electromagnetic pulses, tuned to the Larmor frequency of hydrogen. The pulses are emitted by the sender and receiver coil, sitting in the centre of the probe head. By moving the probe head in respect to a sample using a

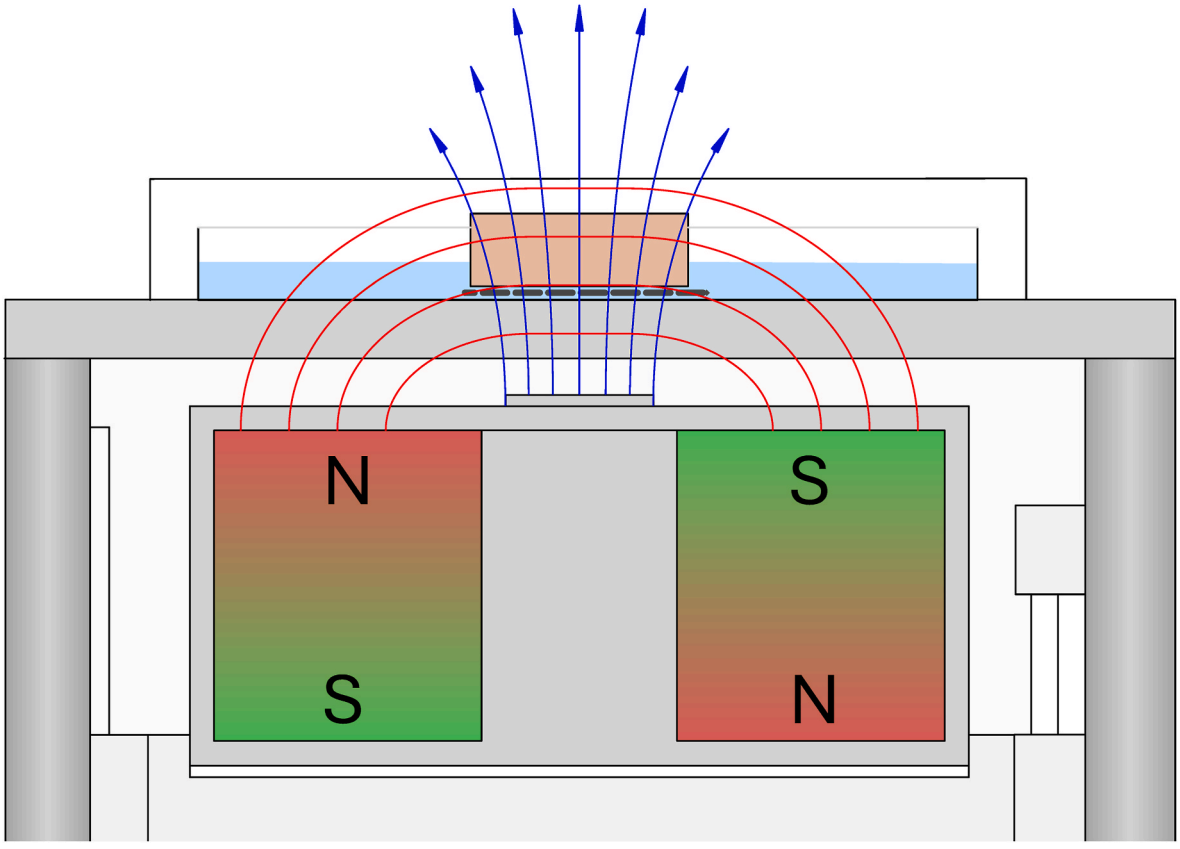

Fig. 7. Schematic drawing of the NMR device and the test setup for dissolution tests.

high precision step motor, a depth profile is obtained. The technique is entirely non-destructive and allows the repeated measurement of a single sample over time up to a depth of several millimetres. No extra preparation altering the sample is necessary as water is the probing substance itself. Measurements are done using a CPMG pulse sequence with the parameters as described in Table 2 with a more elaborate description of parameters found in (Blümich, 2000; Schulte Holthausen et al., 2022). This way, two independent parameters can be detected by the NMR device: First, the signal amplitude at first excitation is a measure of the proton density and thus, a direct measure of the volumetric water content. It has been shown that after appropriate signal correction of the first echo and subsequent signal normalization to liquid water, this allows the quantification of the water filled porosity Φ_{NMR} (Schulte Holthausen and Raupach, 2018, 2021). Second, the exponential attenuation of the signal, the so-called T_2 relaxation, allows the estimation of corresponding pore sizes.

First, samples are placed on the NMR device and a profile is measured in its preconditioned state. Second, the sample is placed on the device onto a felt cloth within a glass Petri dish with only 2 mm thickness. Water is poured into the Petri dish, and the repeated measurement is started immediately. To prevent excessive water evaporation during the experiment, the Petri dish is covered with a plastic lid. Fig. 7 shows the test setup. For any NMR profile, a CPMG sequence is applied every millimetre slightly before the surface of the sample at 3 mm up to 10 mm depth.

For evaluation, the exponentially decaying CPMG echoes are fitted using a bi-exponential, non-negative linear least-squares algorithm as described by the following Equation 4

$$\left[\left(echo(t) - \sum_{n=1}^{2} A_n * e^{\left(-\frac{t}{T_{2n}}\right)}\right)^2\right]_{min} \quad \text{Eq. 4}$$

The two individual T_2 relaxation times are bound between a shortest possible T_2 of the echo spacing time as a lower limit and the relaxation time of water $T_{2,w}$ due to diffusive attenuation (Schulte Holthausen and Raupach, 2019).

3. Results from conventional building material testing

3.1. Water content and compressive strength

The results of compression testing on earthen bricks are shown in Fig. 8, along with the water content of the samples after preconditioning in the respective climates. The dots represent the mean value of the compressive strength, with the maximum and minimum represented by the "whiskers". The triangles display the water content in relation to the dried state at 105 °C. For each humidity level, three samples are tested.

The compressive strength rises as the relative humidity and water content lower. The strength at 90 % RH is about 37 % lower than at 50 % RH. The oven-dried samples reach a compressive strength that is 50 % higher than 11.4 N/mm² at 50 % RH. The linear correlation, postulated by (Brinkmann and Whiele, 2023) applies to those two mean values. Considering the variation, we find not a linear correlation, but rather a root-RH correlation between 50 % RH and 90 % RH, since the measured values are higher than postulated. The coherence between the relative humidity and water content of the samples tends to be non-linear. In summary it is evident, that a higher relative humidity in preconditioning leads to a higher water content, which results in a reduced compressive strength.

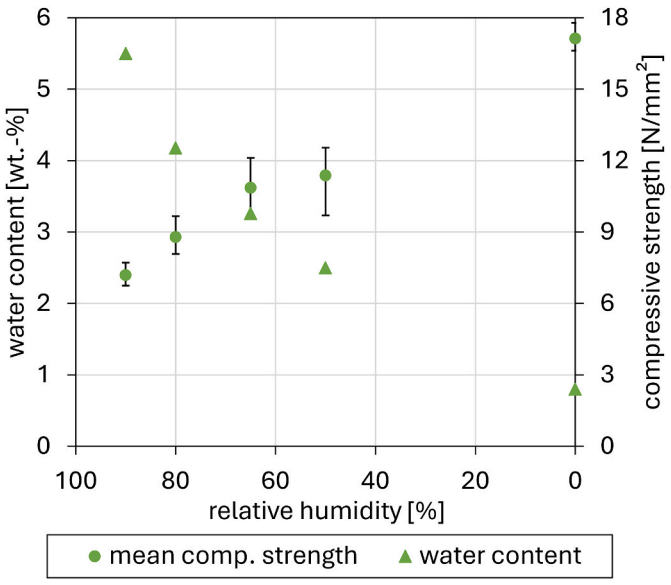

Fig. 8. Compressive strength of earthen bricks with varying storage climate.

Table 2
^{1}H NMR measurement parameters employed in this study.

	Parameter	Unit	Value
CPMG	Larmor frequency	MHz	13.1
	Pulse length	µs	16
	Echo spacing time	µs	81
	Number of echoes		100
	Acquisition window	µs	16.5
	Deadtime	µs	24.5
	Recycle delay	ms	1000
	Number of scans	–	128
	Magnetic field gradient	kHz/mm	300
Normalization	Signal intensity of water A_W	–	235
	Correction divisor 1st echo	–	0.75
	Correction divisor 2nd echo	–	1.00
	Relaxation time of water $T_{2,w}$	ms	125

3.2. Capillary water absorption

The water absorption in litres per square meter is displayed as a function of the square root of time in Fig. 9 (left). To account for the different stone humidities at the start of the study due to the conditioning, the graphs of samples conditioned in 50 % RH and 65 % RH start at a water absorption of 1.5 and 2.0 l/m. These values are calculated as the difference the gently dried mass at 40 °C and the equilibrium humidity in accordance with (b).

Initially, the samples with 65 % RH exhibit the highest water absorption due to their conditioning, which is considered in this observation. After 1 h, the water absorption of the 50 % RH sample is equal to the absorption of the longitudinal sample conditioned at 65 % RH. After 24 h, the samples begin to group according to their direction of measurement rather than the pre-test conditioning. The observations in the water absorption graphic can be transferred into the capillary water absorption coefficient, as seen in Fig. 9 right. Although the correlation does not appear strongly linear, the water absorption is determined using Eq. (3) in the interval from the starting point to 1 h and from the starting point to 24 h. The samples measured longitudinal to the direction of extrusion (L), have a water absorption coefficient, which is about 10 %–30 % above the coefficient of the samples measured orthogonal to the direction of extrusion (O). This indicates a more distinctive capillary pore structure longitudinal to the direction of extrusion than orthogonal.

Considering the preconditioning, a connection of water content before testing and water absorption can be observed. The greater the water content of the sample due to preconditioning, the slower the water absorption within 24 h. During the first hour, this correlation appears to be influenced by other uncertainties that may arise from measurement inaccuracies. These inaccuracies lead to a higher water adsorption in the sample 20–65 L after 1 h compared to after 24 h.

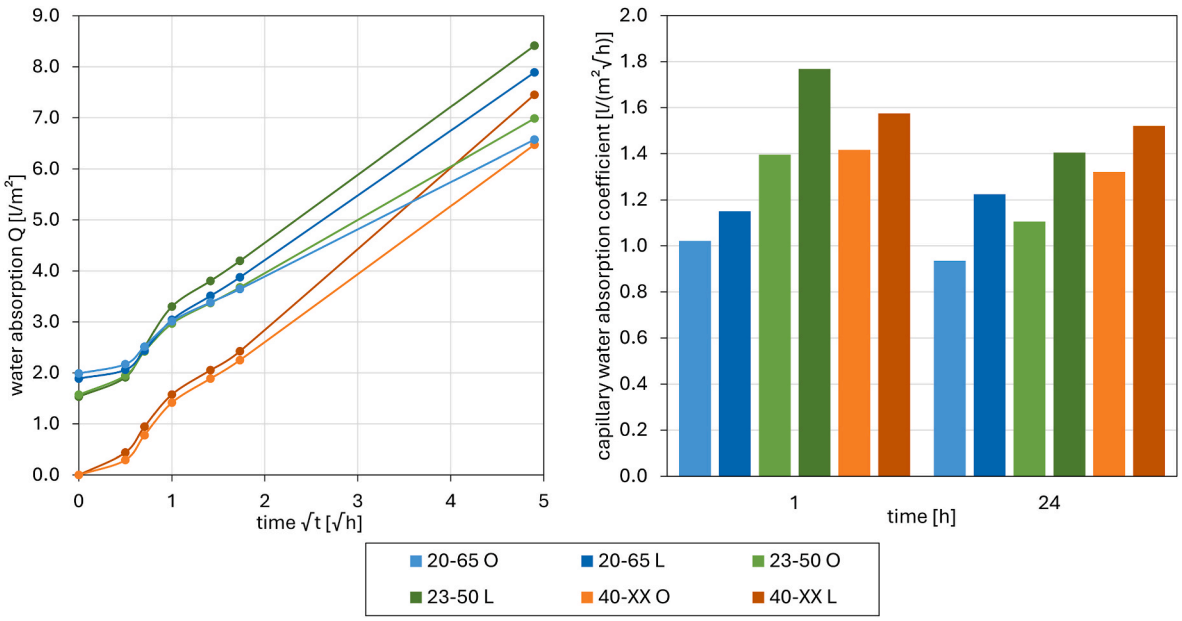

Fig. 9. Left: capillary water absorption as a function over time, **right:** capillary water absorption coefficient after 1 and 24 h.

These deviations are explained by two causes; (i) at the first stages of the measurement procedure a water layer adsorbed to the sample by surface tension which cannot be swabbed off and (ii) due to the loss of material. The rising water content at the surface leads to a replastification of the earthen material which leads to detachments on the wettened surface of the sample. Within the 24 h of water immersion no significant detachments are observed due to extremely careful sample-handling. Nevertheless, a slight discoloration of the underlying tile occurres due to material residues. In this case individual values are determined. A larger number of samples would be required to better account for the scattering.

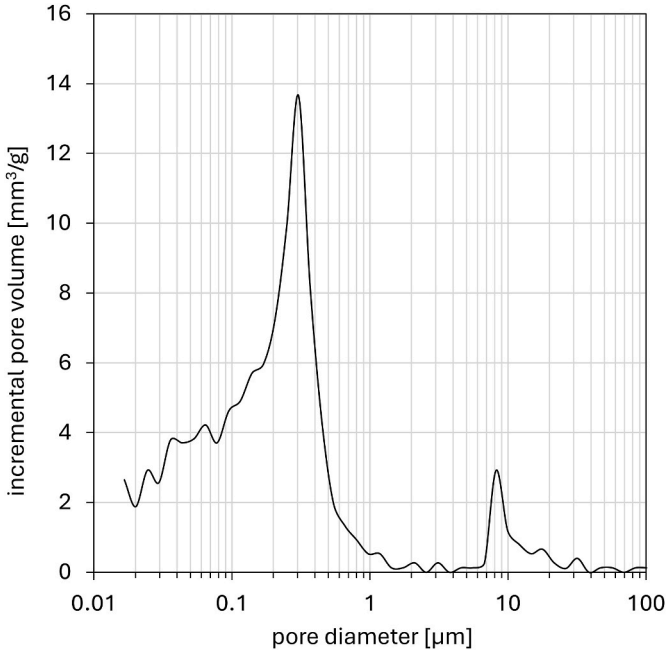

Fig. 10. Pore size distribution of the vacuum-extruded earthen blocks.

3.3. *Mercury porosimetry*

As Fig. 10 shows, the pore space can be divided into two groups, one ranging from 20,000–3000 nm the other ranging from 700 to 8 nm, with the second one being the more significant one with a ratio of about 92 % of the cumulative pore volume. The overall porosity adds up to 22 vol.-%.

The pore spaces cannot be separated into different orientations of the pores, which is why the thesis of a more distinctive pore structure longitudinal to the direction of extrusion than orthogonal cannot be further examined here. In addition, mercury porosimetry can only be used on the material in a dried state. To describe the behaviour of earthen materials when exposed to water, including the swelling process of the clay particles, further investigations with other methods are needed. To get a detailed view while the water absorption takes place, nuclear magnetic resonance measurements are employed.

4. Results from single-sided ^{1}H nuclear magnetic resonance

4.1. *CPMG relaxation response on swollen samples*

Fig. 11 presents the CPMG echo decay curve of a representative sample after 10 h of water immersion, during which swelling occurred. The data clearly exhibit two distinct fit components, and the figure demonstrates both the high quality of the measurements and the adequacy of the bi-exponential fit used to model the signal decay. As discussed in more detail later, the shorter relaxation component, characterised by an amplitude of 27.8 % and a T_2 relaxation time of 1.3 ms, is attributed to water located within the interlayer spaces of the highly swollen clay particles. The parameters of this component are hereafter referred to as A_{IL} and T_{2_IL}, respectively. These values are in good agreement with literature reports for interlayer water under similar conditions [(Fleury et al., 2013); (Eizaguirre et al., 2024)]. The longer relaxation component, characterised by an amplitude of 11.7 % and a T_2 relaxation time of 7.5 ms, is attributed to water located in between clay particles (interparticle). The parameters of this component are hereafter referred to as A_{IP} and T_{2_IP}, respectively. The clear differentiation of two individual signal components, as seen here is not necessarily expected based on past studies on clay (Fleury et al., 2013) and likely a result of the high water-to-clay-binder ratio developing during the continuous swelling experiments.

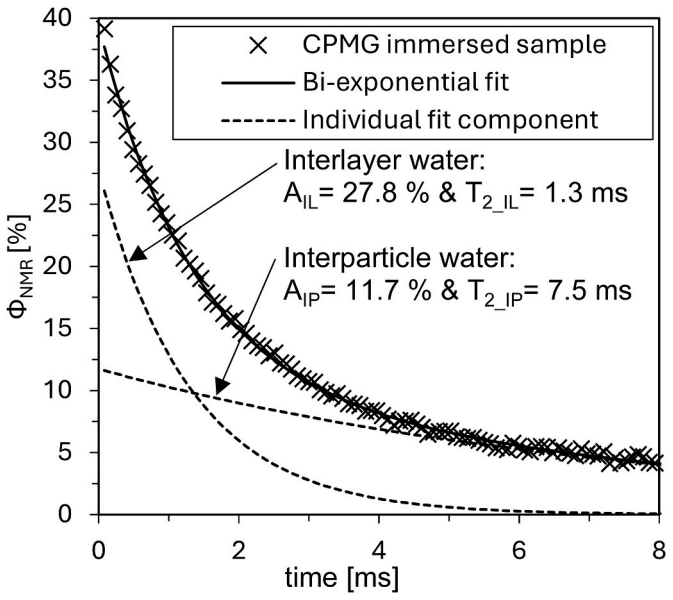

Fig. 11. CPMG from sample 0–28 preconditioned at 20 °C/80 % RH after 10 h of immersion with signal averaged between 8 and 10 mm depth within the sample.

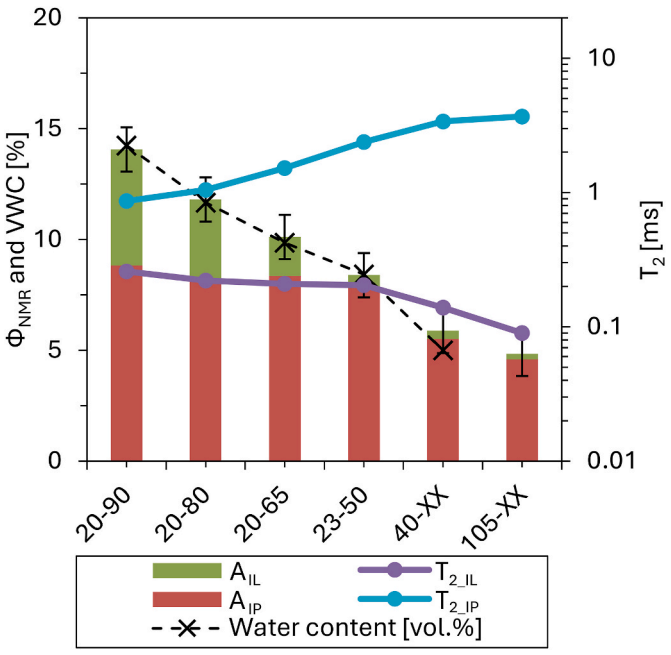

Fig. 12. NMR signal from earthen blocks after storage at different climates with a differentiation between interlayer (A_{IL} and T_{2_IL}) and interparticle (A_{IP} and T_{2_IP}) water shown as cumulative signal stagged onto each other. Additionally, the gravimetrically measured volumetric water content (VWC) is shown.

Additionally, a minor signal deviation in the first echo, appearing significantly above the fitted curve, is attributed to residual hydroxide-bound water, which exhibits a very short T_2 relaxation time. Previous studies have shown that single-sided ^{1}H NMR devices tend to enhance and prolong signals from solid phases such as hydroxides, in contrast to conventional closed magnet systems (Schulte Holthausen and McDonald, 2020). This effect is likely due to the specific pulse sequences used in the highly inhomogeneous magnetic fields (Schulte Holthausen and Raupach, 2019). However, any attempt to quantify this relaxation component is deemed infeasible.

Paramagnetic iron strongly enhances surface relaxation in porous materials and thus, shortens the detected relaxation for otherwise similar sized pores (Schulte Holthausen and Raupach, 2019). If the amount of iron estimated for the samples of around 6 wt.-% would all contribute to NMR surfacy relaxivity, a considerably faster relaxation would be expected than found here. Consequently, it might be assumed that most iron within the samples here is bound in concentrated spots, possibly unhydrated. Only a limited amount of iron is evenly distributed throughout the pore systems contributing to surface relaxation.

4.2. Preconditioned sample measurement

Fig. 12 displays the fitted results from NMR measurements of all samples, preconditioned under different climatic conditions. As in the swollen samples (see Fig. 11), two relaxation components adequately describe the decaying CPMG signal; however, the T_2 relaxation times observed here are significantly shorter. As expected, more severe drying, achieved either by lowering the relative humidity or increasing the temperature, leads to a reduction in sample water content, reflected in a decreased total NMR amplitude Φ_{NMR}. When transitioning from a conditioning climate of 20 °C/90 % RH to 23 °C/50 % RH, the amplitude of the interparticle signal A_{IP} declines from approximately 5 % to nearly zero, while the corresponding relaxation time T_{2_IP} increases gradually from 1 ms to 3 ms. The latter behaviour may be attributed to the increasing isolation of larger pore spaces from smaller, faster-relaxing clay particle surfaces, and the reduction of water mobility and water connectivity. Alternatively, this trend might arise from the bi-exponential fitting approach, which becomes more susceptible to measurement noise at low signal amplitudes and may artificially extend T_2 values. Therefore, the interpretation of increasing T_{2_IP} should be approached with caution when A_{IP} is relatively small. The shorter relaxation component, corresponding to interlayer water A_{IL}, remains more stable, with amplitudes around 8 % and T_2 relaxation times near 0.2 ms. Only under more extreme drying conditions, such as heating to 105 °C, is this component significantly reduced, with T_{2_IL} decreasing to approximately 0.09 ms.

Comparing the results from ^{1}H NMR on the preconditioned samples and the compression strength measurements in Fig. 8, the importance of the interparticle water A_{IP} to the structural integrity of the earthen building materials is emphasized. An increase in interparticle water appears to strongly reduce material strength.

The NMR-derived data are overlaid with gravimetric measurements of volumetric water content. To align these datasets, an arbitrary offset of 5 % is added to the gravimetric values. This accounts for e.g. weight changes that are not detectable by NMR. This adjustment helps to illustrate the strong correlation between gravimetrically determined water content and Φ_{NMR}. This supports the validity of the applied correction and normalization procedure for using Φ_{NMR} as a proxy for volumetric water content, as previously demonstrated (Schulte et al., 2018, Schulte Holthausen and Raupach, 2021). However, beyond 40 °C drying, increasing discrepancies emerge between Φ_{NMR} and gravimetric values, possibly due to the loss of water associated with other hydrated phases or hydroxides that are not, or only partially, detectable by NMR.

4.3. Time-dependent progression of swelling reactions

To examine the temporal evolution of water binding within the clay binder, the NMR relaxation signal gets averaged over a depth range of 8–10 mm and analysed over immersion time. Results for four representative samples are presented in Fig. 13. As expected, all samples exhibit a sharp increase in signal shortly after initial immersion in water, reflecting rapid water absorption into the material. During the first hour, A_{IL} increases, followed by a subsequent rise in A_{IP}. Interestingly, this sequence is in marked contrast to the behaviour observed in internally swelling calcium–silicate–hydrate (C–S–H) phases in cementitious materials (Schulte Holthausen and Raupach, 2018; M Gajewicz et al., 2016). The time-resolved evolution of the relaxation components clearly

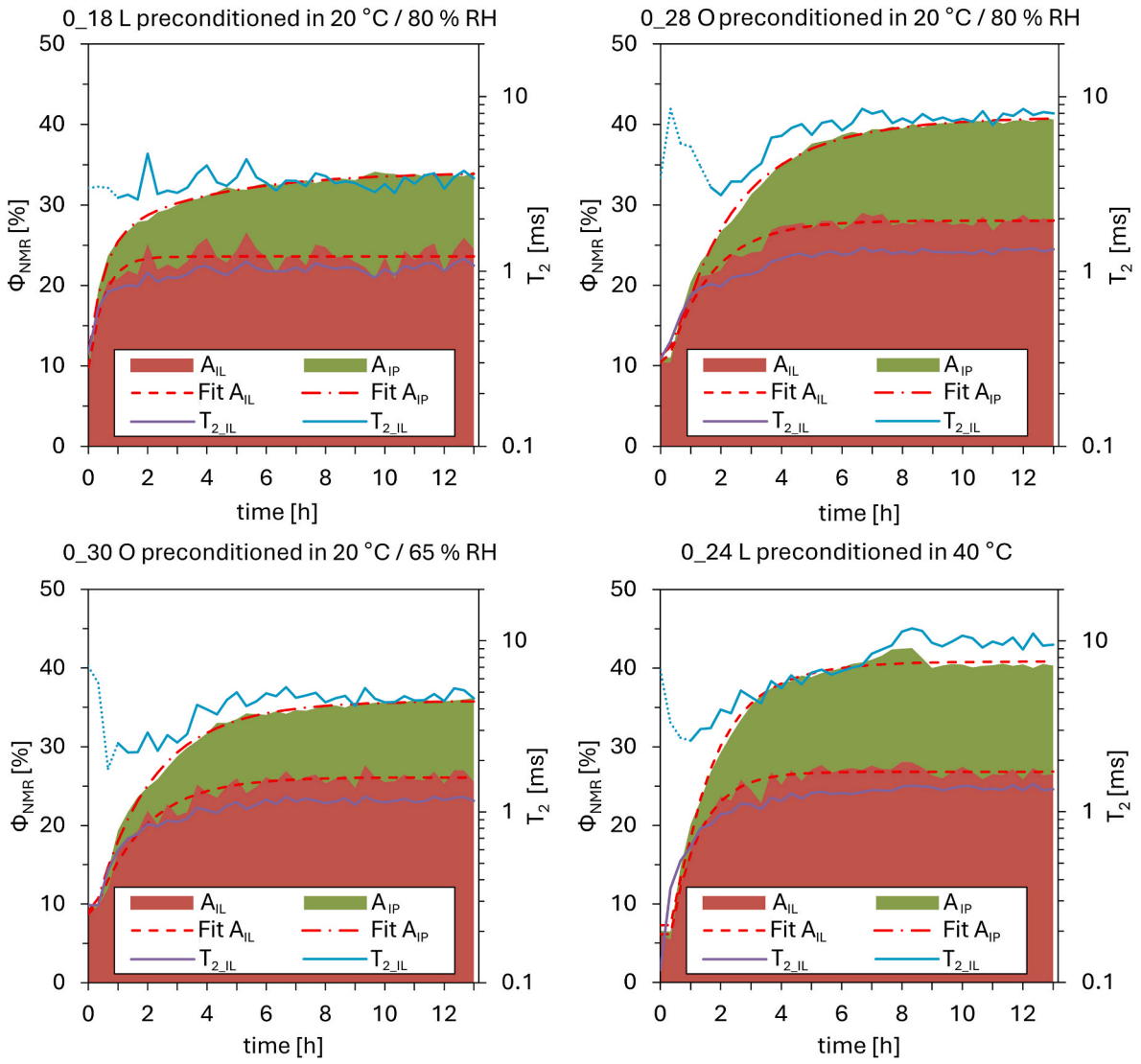

Fig. 13. Change in water binding in samples while water immersion and dissolution in a depth of 8–10 mm.

shows that the two distinct components identified in the swollen state (Fig. 11) evolve continuously from the two shorter components observed in the preconditioned dry samples (Fig. 12). Specifically, the relaxation time T_{2_IL}, which initially ranges from 0.1 to 0.2 ms (see Fig. 12), progressively increases to approximately 1.3 ms, while its associated amplitude A_{IL} rises to about 25 %. This behaviour is consistent with previous studies on clays subjected to controlled wetting conditions (Eizaguirre et al., 2024).

In contrast, the temporal development of T_{2_IP}, is more challenging to interpret. The bi-exponential fitting algorithm tends to yield unreliable T_2 values when the corresponding amplitude A_{IP} is very low. In Fig. 13, such uncertain T_{2_IP} values—associated with low Amplitudes A_{IP}—are indicated by grey lines. Nevertheless, a general increase in T_{2_IP} is observed over time, eventually reaching values between 3 and 10 ms.

To quantify the temporal changes, and thereby the degradation processes, occurring within the swelling clay samples, an empirical fitting approach is applied to the evolution of the NMR signal amplitude, as described by Equation (3):

$$A_{IL,IP}(t) = A_{IL,IP;ini} + \max\left(0; \left(A_{IL,IP;fin}\text{-}A_{IL,IP;ini}\right) * \left(1\text{-}\exp\left(-\frac{t\text{-}t_{IL,IP;0}}{\vartheta_{IL,IP}}\right)\right)\right) \quad \text{Eq. 3}$$

In this equation, A represents the signal amplitude in % of interlayer A_{IL} and interparticle A_{IP} components over time t in hours, with A_{ini} and A_{fin} denoting the initial amplitude at time zero and the final amplitude at the end of measurement at 12.5 h, respectively. The parameter t_0 accounts for the delay in swelling associated with the time required for the water front to reach the evaluated sample depth range of 8–10 mm. Most importantly, $\vartheta_{IL,IP}$ are the time coefficients characterising the temporal change in the signal. A smaller value of ϑ indicates faster swelling of the clay matrix, and vice versa. This fitting function is intended solely as a means of empirically describing the observed data and extracting quantitative indicators from the temporal signal development. It carries no underlying physical interpretation and should not be viewed as a mechanistic model. The resulting fitting curves are indicated in Fig. 13 as dotted red lines and the extracted time coefficients are presented in Fig. 14.

It is evident that the interlayer time coefficient is consistently smaller than the interparticle time coefficient, indicating that interlayer swelling occurs on a shorter timescale than the swelling associated with interparticle water. However, the relative timing of these processes depends strongly on the preconditioning conditions. Under more severe drying, the interlayer and interparticle swelling processes occur in close succession. In contrast, preconditioning at higher humidity significantly accelerates interlayer swelling while delaying the onset of interparticle swelling.

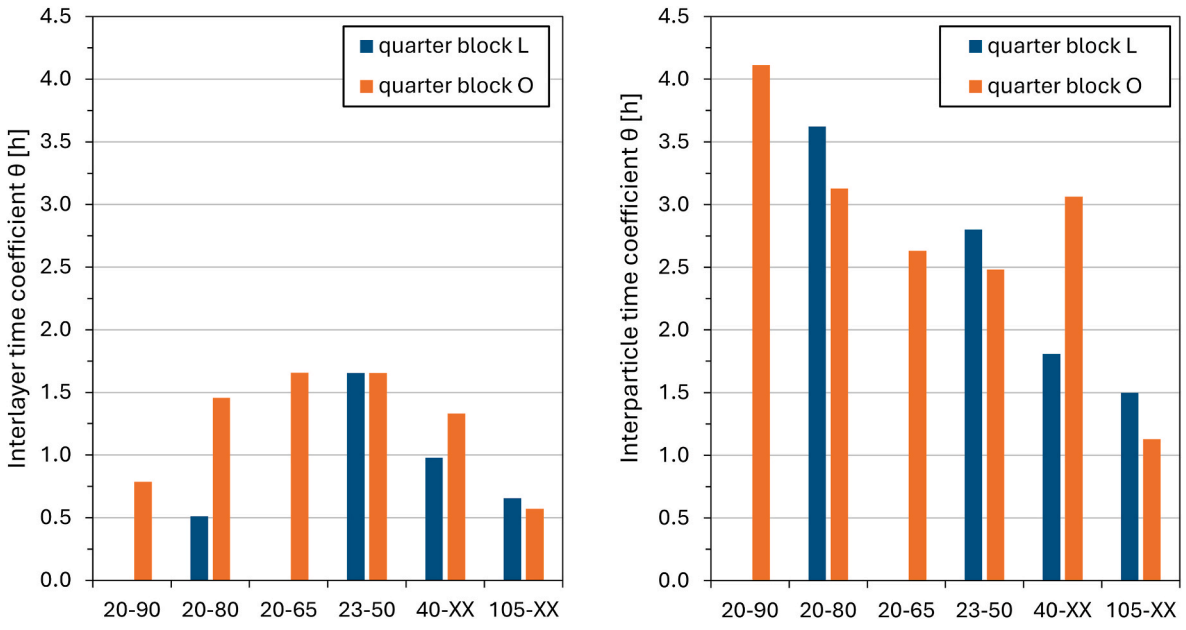

Fig. 14. Time coefficients ϑ_{IL} and ϑ_{IP} of interlayer and interparticle changes, respectively, acc. to Equation 3.

Comparing these results with the found CWA (see section 3.3 and section 4.4), a closer connection between CWA and interparticle swelling can be observed, despite of an overall greater signal increase, and thus water absorption and storage within the sample, for interlayer signal.

4.4. Implications of swelling depended relaxation signal on surface relaxivity

1An additional insight can be drawn from the connection between the interlayer signal amplitude A_{IL} and its corresponding relaxation time T_{2_IL}, shown in Fig. 15. As A_{IL} increases, a proportional increase in T_{2_IL} is consistently observed. This strong correlation is illustrated in Fig. 6 for all samples, revealing two distinct linear regimes with different slopes above and below a T_{2_IL} value of approximately 0.9 ms. The observed correlation is likely attributable to a constant inner surface area and surface relaxivity of the clay particles. As more water layers are incorporated into the interlayer space, both the NMR signal amplitude and T_2 relaxation time increase, corresponding to an expansion of the interlayer spacing. The inflection point around T_{2_IL} of 0.9 ms suggests a transition in the water-binding regime, from a structured, layer-like arrangement to a more disordered, diffuse ionic layer. This transition alters the mobility of water molecules and their interaction with the clay surfaces and consequently affects surface relaxivity.

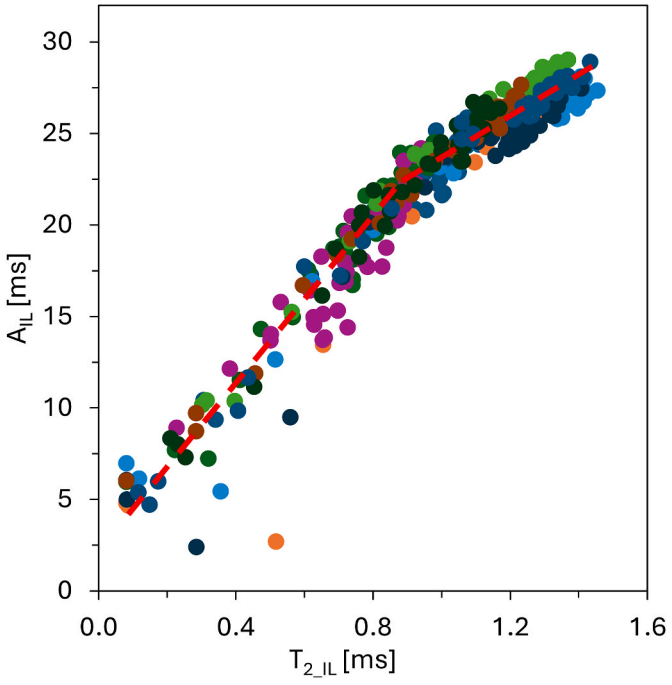

Fig. 15. Correlation between interlayer amplitude A_{IL} and its corresponding relaxation time T_{2_IL}. The red dotted line serves as guide to the eye.

While absolute values for surface relaxivity cannot be drawn from this data without considerable assumptions, the changes in slope at the inflection point suggests that surface relaxivity of the distorted, diffuse ionic layer (above $T_{2\_IL} = 0.9$ ms) is only about 1/3 of surface relaxivity of the more structured, layer like arrangement (below $T_{2\_IL} = 0.9$ ms). Interestingly, Eizaguirre et al. (2024) propose just such change in surface relaxivity, though at a different water content of 30 % and different T_2 relaxation time of ~0.3 ms. The change in slope found is by 1/5. In respect to the differences in clay materials (inner surface, paramagnetic impurities etc.) investigated here and in their study, it is noteworthy that these results comply such well. Even more so, revisiting the results presented by Eizguirre et al. (Eizaguirre et al., 2024), reinterpreting the single highest data point (amplitude of 52 % and 2.4 ms) as an outlier, and ignoring it in the subsequent linear regression, a similar change of slope of 1/3 with an inflection point of ~28 % can be inferred.

The strong linear relationship between A_{IL} and T_{2_IL} supports the general applicability of the fast diffusion model for interlayer water in these systems. In contrast, no such correlation is observable for the interparticle water component (data not shown), indicating differing relaxation mechanisms or geometries in those environments.

4.5. Capillary water absorption

The degradation of earthen building materials due to water exposure remains one of the primary challenges limiting their broader adoption, despite their environmental advantages. A critical parameter for evaluating such materials in an engineering context is the capillary water absorption (CWA), along with the derived capillary water absorption coefficient (CWAC). Using ^{1}H nuclear magnetic resonance (NMR)

profiling, water absorption can be monitored non-destructively. Fig. 16 presents the moisture profiles of a sample preconditioned at 20 °C and 80 % RH, recorded at four different time intervals. As expected, water penetration initiates at the exposed surface, depicted on the left side of each panel, and advances further into the material over time. Concurrently, the previously discussed swelling behaviour is observed, characterised initially by an increase in the interlayer signal A_{IL}, followed subsequently by a rise in the interparticle signal A_{IP}.

To quantify this process, water absorption is determined using a method analogous to that employed for natural stones (Keine et al., 2019). This involves calculating the volumetric water absorption of the sample, accounting for the initial moisture content of the preconditioned sample. A linear approximation of the NMR signal Φ_{NMR} is used, beginning at the sample surface at a depth of 4 mm. The resulting water absorption is represented as the blue triangular area in Fig. 16. Initially, this water addition remains within the measurable range, but after only a few time points, it extends beyond the field of view. The increase in water content is indicated by the blue triangles in Fig. 16, whose areas represent the temporal water absorption (TWA) and are plotted in Fig. 17 left.

As expected for capillary water absorption experiments, the absorption follows a square-root-of-time dependence, appearing linear when plotted against the square root of time. In this analysis, three samples exhibit significantly higher CWA, likely due to macroscopic cracking caused by preconditioning at elevated temperatures and the subsequent swelling in water. The capillary water absorption coefficient (CWAC), calculated via linear regression between 20 and 100 min (1.3 $h^{0.5}$), is presented in Fig. 17 right. An increase in CWAC is observed with more severe preconditioning at higher temperatures. This trend is consistent with previous measurements of CWAC on conventionally tested samples, as discussed in Section 3.2, with overall comparable values, especially at 50 % RH and 65 % RH. The samples dried at 40 °C indicate a higher CWAC in NMR testing, than in conventional methods. This may occur due to the different setup. While in case of the conventional testing the samples are placed on top of a wet cloth, in the NMR measurements the water is about 1 cm on the sample to provide sufficient water for the time of testing. To be able to accurately test the CWAC on severely dried stones, the test setup could be modified by

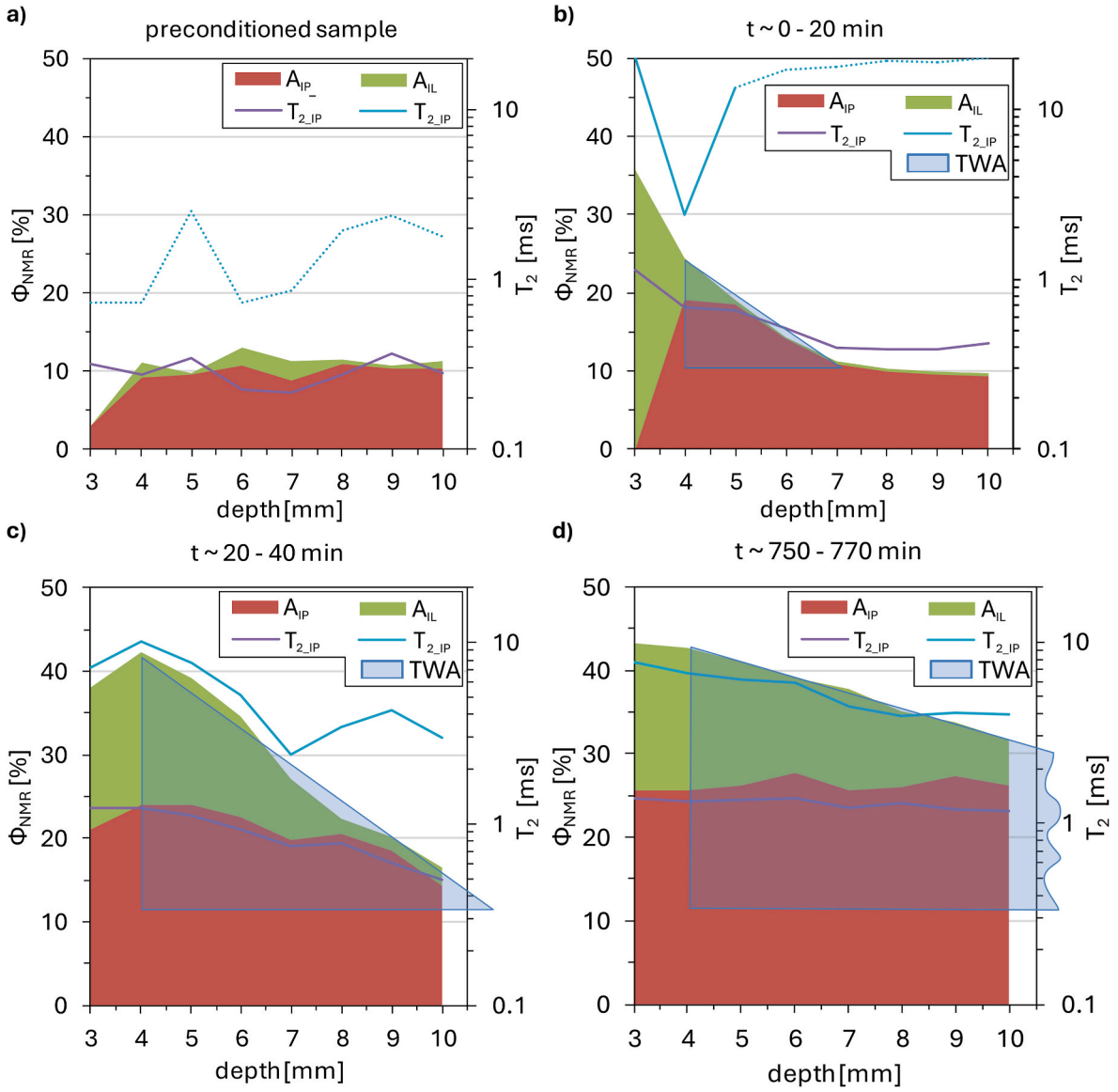

Fig. 16. NMR profiles of earth-based sample water content in capillary absorption experiment **a)** of the sample after preconditioning at 20 °C and 80 % RH before immersion, **b)** after immersion within the first 20 min, **c)** within 20 and 40 min and **d)** after about 12 h. NMR signal is split into interlayer (A_{IL}) and interparticle (A_{IP}) with its corresponding T_2 relaxation times. Blue rectangles indicate the increase in water content as evaluated for the capillary water absorption evaluation.

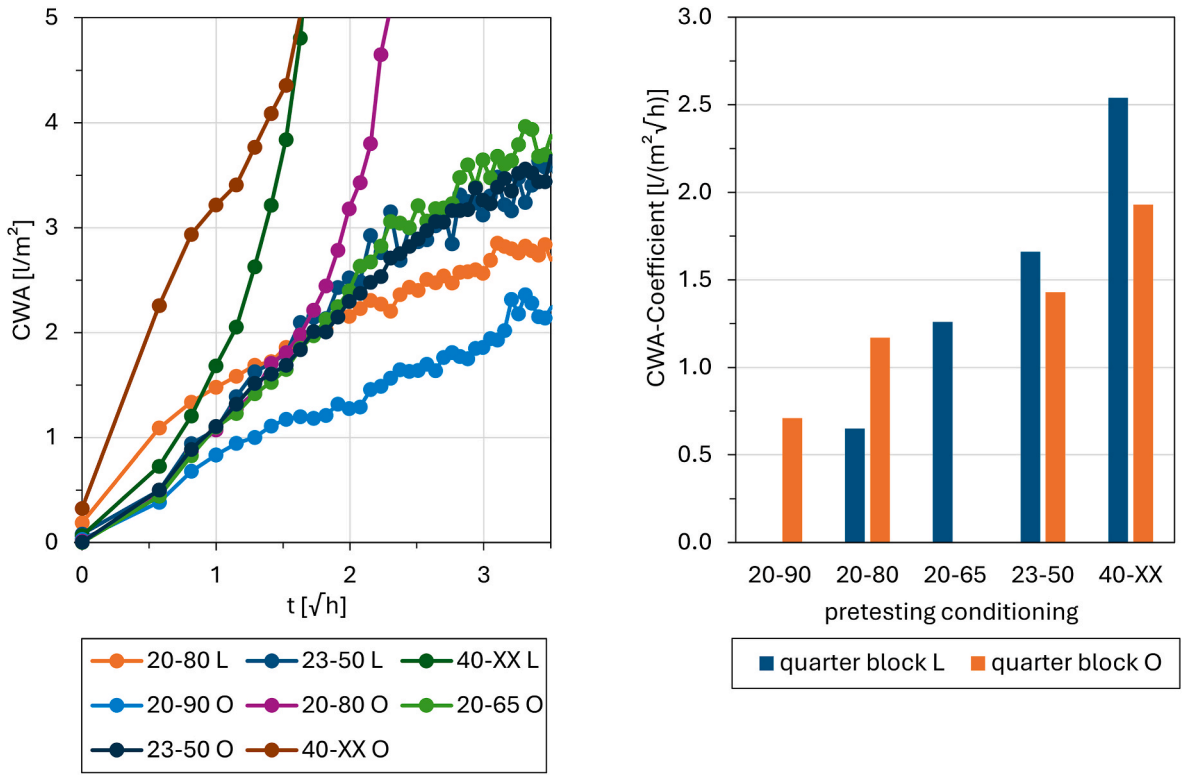

Fig. 17. Capillary water absorption derived from NMR measurements as **left:** time-dependent capillary water absorption; **right:** evaluated as capillary water absorption coefficient for all samples.

using an external water reservoir.

5. Conclusions

The testing of earth-based blocks using single-sided ^{1}H nuclear magnetic resonance yields reasonable results. It allows the depth wise visualisation of water absorption. The results of this new testing method together with the conventional testing methods can be summarized as follows:

- The pore distribution and, therefore, the pathways for capillary water absorption in vacuum-extruded blocks depend on the direction of extrusion. Water absorption parallel to the direction of extrusion is greater than that occurring orthogonally. By employing single-sided NMR, it is possible to obtain depth-dependent information regarding the pore structure and the alignment of these pores.
- The swelling of the clay binder can be differentiated into interlayer and interparticle processes, both of which can be quantified and characterised over time. Furthermore, this work provides additional insights into the interaction of water molecules with the surrounding surfaces of clay particles, as observed through ^{1}H nuclear magnetic resonance. The technique enables the visualisation of the transition of water binding from a structured, layer-like arrangement to a more disordered, diffuse ionic layer.
- Capillary water absorption can be detected non-destructively using NMR. The preparation of samples into a manageable size is rendered unnecessary. In contrast to conventional testing methods, depth-dependent analysis is feasible.
- The results at 65 % RH and 50 % RH indicate that the CWAC demonstrates that ^{1}H nuclear magnetic resonance measurements on earthen blocks are practical and yield results comparable to conventional testing methods, with depth-dependent analysis being possible exclusively through this novel technique.

NMR testing helps to understand the swelling properties of earthen blocks and contributes to a realistic pore and water transport model for earthen building materials. Furthermore, single-sided nuclear magnetic resonance testing can be used as an in-situ method for housing construction in cases of building investigations after damage events.

CRediT authorship contribution statement

Florian Soßna: Investigation, Methodology, Visualization, Writing – original draft. **Robert Schulte Holthausen:** Methodology, Visualization, Writing – original draft. **Jeanette Orlowsky:** Supervision, Writing – review & editing.

Declaration of competing interest

The authors declare that they have no known competing financial interests or personal relationships that could have appeared to influence the work reported in this paper.

Acknowledgements

We would like to thank the Brick and Tile Research Institute Essen, Germany for its support in producing the extruded test specimens.

Data availability

Data will be made available on request.

References

Bender, W., 2007. Types of extrusion units. In: Händle, F. (Ed.), Extrusion in Ceramica. Springer, Berlin Heidelberg, pp. 59–84. https://doi.org/10.1007/978-3-540-27102-4.

Berker, E., Albus, J., Soßna, F., Orlowsky, J., 2025. Untersuchungen von stranggepressten Hochlochlehmsteinen als Alternative für Innenwandkonstruktionen, Eng.: investigations of extruded vertically perforated earth bricks as an alternative for

interior wall constructions. ce/papers 8, 120–133. https://doi.org/10.1002/cepa.3296.
Blümich, B., 2000. NMR Imaging of Materials. Clarendon Press, Oxford.
Brinkmann, M., Whiele, P., 2023. Correlation between relative humidity and the strength and deformation characteristics of unstabilised earth masonry. Constr. Build. Mater. 366, 130048. https://doi.org/10.1016/j.conbuildmat.2022.130048.
Brownstein, K.R., Tarr, C.E., 1979. Importance of classical diffusion in NMR studies of water in biological cells. Phys. Rev. 19 (6), 2446–2453.
Calatan, G., Hegyi, A., Dico, C., Mircea, C., 2017. Experimental research and the recyclability of the clay material used in the fabrication of adobe bricks type masonry units. Procedia Eng. 181, 363–369. https://doi.org/10.1016/j.proeng.2017.02.402.
Carr, H.Y., Purcell, E.M., 1954. Effects of diffusion on free precession in nuclear magnetic resonance experiments. Phys. Rev. 94 (3), 630–638.
Casanova, F., Perlo, J., Blümich, B., 2011. Single-Sided NMR. Springer, Heidelberg.
Chauhan, R., Kumar, R., Diwan, P.K., Sharma, V., 2020. Thermogravimetric analysis and chemometric based methods for soil examination: application to soil forensics. Forensic Chem. 17, 100191. https://doi.org/10.1016/j.forc.2019.100191.
DIN 18940: 2023-06, Load Bearing Earth Block Masonry – Construction, Design and Execution.
DIN 18945: 2024-03, Earth Blocks – Requirements, Test and Labelling.
DIN EN 15801: 2010-04, Conservation of Cultural Property – Test Methods – Determination of Water Absorption by Capillarity.
DIN EN 17685-1: 2023-04, Earthworks – Chemical Tests – Part 1: Determination of Loss on Ignition.
DIN EN 772-1, 2016. Methods of Testing for Masonry Units – Part 1: Determination of Compressive Strength.
Eizaguirre, P., Tang, A.M., Maillet, B., Sidi-Boulenouar, R., Talandier, J., Pereira, J.-M., Vu, M.N., Chabot, B., Dangla, P., Bornert, M., Aimedieu, P., 2024. Exploring two regimes of water mobility in unsaturated expansive clay using NMR relaxometry. Appl. Clay Sci. 251, 107324. https://doi.org/10.1016/j.clay.2024.107324.
eurostat, 2022. Waste statistics. https://ec.europa.eu/eurostat/statistics-explained/index.php?title=Waste_statistics#Waste_generation_excluding_major_mineral_waste. (Accessed 3 June 2025).
Fleury, M., Kohler, E., Norrant, F., Gautier, S., M'Hamdi, J., Barré, L., 2013. Characterization and quantification of water in smectites with low-field NMR. J. Phys. Chem. C 117, 4551–4560. https://doi.org/10.1021/jp311006q.
Göhlert, K., Uebel, M., 2007. Test methods for plasticity and extrusion behaviour. In: Händle, F. (Ed.), Extrusion in Ceramica. Springer, Berlin Heidelberg, pp. 354–362. https://doi.org/10.1007/978-3-540-27102-4.
Jasmund, K., Lagaly, G., 1993. Tonminerale Und Tone, Struktur, Eigenschaften, Anwendung Und Einsatz in Industrie Und Umwelt. Steinkopff, Darmstadt. https://doi.org/10.1007/978-3-642-72488-6.
Keine, S., Schulte Holthausen, R., Raupach, M., 2019. Single-sided NMR as a non-destructive method for quality evaluation of hydrophobic treatments on natural stones. J. Cult. Herit. 36, 128–134. https://doi.org/10.1016/j.culher.2018.07.012.
Kumari, N., Mohan, C., 2021. Basics of clay minerals and their characteristic properties. In: Do Nascimento, G.M. (Ed.), Clay and Clay Minerals. IntechOpen, London, pp. 15–44. https://doi.org/10.5772/intechopen.95640.
M Gajewicz, A., Gartner, E., Kang, K., McDonald, P.J., Yermakou, V., 2016. A 1H NMR relaxometry investigation of gel-pore drying shrinkage in cement pastes. Cement Concr. Res. 86, 12–19. https://doi.org/10.1016/j.cemconres.2016.04.013.
Meiboom, S., Gill, D., 1958. Modified spin-echo method for measuring nuclear relaxation times. Rev. Sci. Instrum. 29 (8), 688–691.
Müller, A., Ziegert, C., Kaiser, C., Röhlen, U., 2013. Eigenschaften industrieller Lehmbauprodukte für den Mauerwerksbau und Verhalten von Lehmsteinmauerwerk, Eng.: properties of industrial clay products for masonry construction and behavior of clay masonry. Mauerwerk 16, 17–28. https://doi.org/10.1002/dama.201200527.
Rose, D.A., 1965. Water movement in unsaturated porous materials. Rilem Bull. 29 (12/65), 119–123.
Schulte Holthausen, R., Merkel, M., Breit, W., Raupach, M., 2022. Monitoring the microstructural deterioration of concrete exposed to leaching in purified water, civil eng. Design 4, 99–109. https://doi.org/10.1002/cend.202100051.
Schulte Holthausen, R., McDonald, P.J., 2020. On the quantification of solid phases in hydrated cement paste by 1H nuclear magnetic resonance relaxometry. Cement Concr. Res. 135, 106095. https://doi.org/10.1016/j.cemconres.2020.106095.
Schulte Holthausen, R., Raupach, M., 2018. Monitoring the internal swelling in cementitious mortars with single-sided 1H nuclear magnetic resonance. Cement Concr. Res. 111, 138–146. https://doi.org/10.1016/j.cemconres.2018.05.021.
Schulte Holthausen, R., Raupach, M., 2019. A phenomenological approach on the influence of paramagnetic iron in cement stone on 2D T1-T2 relaxation in single-sided 1H nuclear magnetic resonance. Cement Concr. Res. 120, 279–293. https://doi.org/10.1016/j.cemconres.2019.03.027.
Schulte Holthausen, R., Raupach, M., 2021. Influence of fresh concrete pressure on cover porosity investigated by single-sided proton nuclear magnetic resonance. Mag. Concr. Res. 73, 45–54. https://doi.org/10.1680/jmacr.18.00495.
Soßna, F., Orlowsky, J., 2025. Influence of additives on the strength and deformation behavior of loam blocks. Buildings 15, 919. https://doi.org/10.3390/buildings15060919.